TESS Reveals HD 118203 b to be a Transiting Planet

The Astronomical Journal, 159:243 (12pp), 2020 June https://doi.org/10.3847/1538-3881/ab84f2

TESS Reveals HD 118203 b to be a Transiting Planet

Joshua Pepper[1], Stephen R. Kane[2], Joseph E. Rodriguez[3], Natalie R. Hinkel[4], Jason D. Eastman[3], Tansu Daylan[5,27], Teo Mocnik[2], Paul A. Dalba[2,28], B. Scott Gaudi[6], Tara Fetherolf[7], Keivan G. Stassun[8], Tiago L. Campante[9,10], Andrew Vanderburg[11,29], Daniel Huber[12], Diego Bossini[9], Ian Crossfield[5,13], Steve B. Howell[14], Andrew W. Stephens[15], E. Furlan[16], George R. Ricker[5], Roland Vanderspek[5], David W. Latham[17], S. Seager[5,18,19], Joshua N. Winn[20], Jon M. Jenkins[14], Joseph D. Twicken[14,21], Mark Rose[14], Jeffrey C. Smith[14,21], Ana Glidden[5,18], Alan M. Levine[5], Stephen Rinehart[22], Karen A. Collins[17], Andrew W. Mann[23], Jennifer A. Burt[24], David J. James[3,25], Robert J. Siverd[26], and Maximilian N. Günther[5,30]

[1] Department of Physics, Lehigh University, 16 Memorial Drive East, Bethlehem, PA 18015, USA
[2] Department of Earth and Planetary Sciences, University of California, Riverside, CA 92521, USA
[3] Center for Astrophysics|Harvard & Smithsonian, 60 Garden Street, Cambridge, MA 02138, USA
[4] Southwest Research Institute, 6220 Culebra Road, San Antonio, TX 78238, USA
[5] Department of Physics and Kavli Institute for Astrophysics and Space Research, Massachusetts Institute of Technology, Cambridge, MA 02139, USA
[6] Department of Astronomy, The Ohio State University, 140 West 18th Avenue, Columbus, OH 43210, USA
[7] Department of Physics and Astronomy, University of California, Riverside, CA 92521, USA
[8] Vanderbilt University, Department of Physics & Astronomy, 6301 Stevenson Center Lane, Nashville, TN 37235, USA
[9] Instituto de Astrofísica e Ciências do Espaço, Universidade do Porto, Rua das Estrelas, 4150-762 Porto, Portugal
[10] Departamento de Física e Astronomia, Faculdade de Ciências da Universidade do Porto, Rua do Campo Alegre, s/n, 4169-007 Porto, Portugal
[11] Department of Astronomy, The University of Texas at Austin, Austin, TX 78712, USA
[12] Institute for Astronomy, University of Hawai'i, 2680 Woodlawn Drive, Honolulu, HI 96822, USA
[13] Department of Physics and Astronomy, University of Kansas, 1082 Malott, 1251 Wescoe Hall Drive, Lawrence, KS 66045, USA
[14] NASA Ames Research Center, Moffett Field, CA 94035, USA
[15] Gemini Observatory, NSF's National Optical-Infrared Astronomy Research Laboratory, Hilo, HI 96720, USA
[16] IPAC, Mail Code 314-6, Caltech, 1200 E. California Boulevard, Pasadena, CA 91125, USA
[17] Harvard-Smithsonian Center for Astrophysics, 60 Garden Street, Cambridge, MA 02138, USA
[18] Department of Earth, Atmospheric and Planetary Sciences, Massachusetts Institute of Technology, Cambridge, MA 02139, USA
[19] Department of Aeronautics and Astronautics, MIT, 77 Massachusetts Avenue, Cambridge, MA 02139, USA
[20] Department of Astrophysical Sciences, Princeton University, 4 Ivy Lane, Princeton, NJ 08544, USA
[21] SETI Institute, Mountain View, CA 94043, USA
[22] NASA Goddard Space Flight Center, Greenbelt, MD 20771, USA
[23] Department of Physics and Astronomy, The University of North Carolina at Chapel Hill, Chapel Hill, NC 27599, USA
[24] Jet Propulsion Laboratory, California Institute of Technology, 4800 Oak Grove Drive, Pasadena CA 91109, USA
[25] Black Hole Initiative at Harvard University, 20 Garden Street, Cambridge, MA 02138, USA
[26] Gemini Observatory, Northern Operations Center, 670 N. A'ohoku Place, Hilo, HI 96720, USA
Received 2019 November 1; revised 2020 March 25; accepted 2020 March 26; published 2020 May 1

Abstract

The exoplanet HD 118203 b, orbiting a bright ($V = 8.05$) host star, was discovered using the radial velocity method by da Silva et al., but was not previously known to transit. Transiting Exoplanet Survey Satellite (TESS) photometry has revealed that this planet transits its host star. Nine planetary transits were observed by TESS, allowing us to measure the radius of the planet to be $1.136^{+0.029}_{-0.028} R_J$, and to calculate the planet mass to be $2.166^{+0.074}_{-0.079} M_J$. The host star is slightly evolved with an effective temperature of $T_{\rm eff} = 5683^{+84}_{-85}$ K and a surface gravity of $\log g = 3.889^{0.017}_{0.018}$. With an orbital period of $6.134985^{+0.000029}_{-0.000030}$ days and an eccentricity of 0.314 ± 0.017, the planet occupies a transitional regime between circularized hot Jupiters and more dynamically active planets at longer orbital periods. The host star is among the 10 brightest known to have transiting giant planets, providing opportunities for both planetary atmospheric and asteroseismic studies.

Unified Astronomy Thesaurus concepts: Exoplanet astronomy (486); Exoplanet systems (484); Transit photometry (1709)

Supporting material: data behind figure

1. Introduction

The dawn of planetary transit science began with the transit detection of planets that had been discovered with the radial velocity (RV) technique. The first of these was HD 209458 b (Charbonneau et al. 2000; Henry et al. 2000) which, for several years thereafter, was the only known transiting planet. To date, there are 11 planets for which transits were detected after an initial RV discovery: HD 80606 b (Fossey et al. 2009; Garcia-Melendo & McCullough 2009; Laughlin et al. 2009), 55 Cancri e (Demory et al. 2011; Winn et al. 2011), GJ 436 b (Gillon et al. 2007), HD 149026 b (Sato et al. 2005), HD 189733 b (Bouchy et al. 2005), HD 17156 b (Barbieri et al. 2007), HD 97658 b (Dragomir et al. 2013), GJ 3470 b (Bonfils et al. 2012), HD 219134 b (Motalebi et al. 2015), and HD 219134 c (Gillon et al. 2017). These transiting exoplanets are important because their host stars are bright, especially relative to the typical hosts of transiting exoplanets

[27] Kavli Fellow.
[28] NSF Astronomy and Astrophysics Postdoctoral Fellow.
[29] NASA Sagan Fellow.
[30] Juan Carlos Torres Fellow

(Kane 2007; Kane et al. 2009). The brighter host stars enable detailed follow-up observations to be carried out to study the planetary atmospheres, such as the Spitzer observations of HD 189733 b (Knutson et al. 2007). The Transit Ephemeris Refinement and Monitoring Survey has continued to observe known exoplanets using photometric and RV techniques to refine orbits and investigate a variety of stellar and planetary signatures (Dragomir et al. 2011, 2012; Kane et al. 2011, 2016; Pilyavsky et al. 2011; Hinkel et al. 2015). For the Transiting Exoplanet Survey Satellite (TESS), a primary goal is the detection of planets transiting bright host stars (Ricker et al. 2015) and the subsequent characterization of the atmospheres of some of those planets (Kempton et al. 2018).

Through analysis of the TESS observation strategy and the known exoplanet demographics, Dalba et al. (2019) predicted that several known RV planets would be discovered to transit. The prediction was consistent with the early TESS discovery of an additional transiting planet in the π Mensae system (Huang et al. 2018), which was already known to have a longer-period planet from earlier RV surveys. However, the large number of RV planets with orbital periods shorter than 10 days provides many opportunities to detect further transits among the known RV population (Kane & von Braun 2008). This paper reports the detection of transits of HD 118203 b, a previously known giant planet ($M_p \sin i = 2.17\ M_J$) in a 6.13 day eccentric ($e = 0.31$) orbit around a bright ($V = 8.05$) star (da Silva et al. 2006b). The star was observed by TESS during Sectors 15 and 16 of Cycle 2 observations of the northern ecliptic hemisphere.

The stellar brightness of HD 118203 combined with the eccentric nature of the orbit presents an important opportunity to study the atmospheres of exoplanets under tidal stress from the host star. HD 118203 b joins TOI-172 b (Rodriguez et al. 2019) and HD 2685 b (Jones et al. 2019) as TESS-detected giant planets in eccentric orbits close to their host stars. In Section 2 we describe the details of TESS observations and photometry, as well as ground-based observations that contribute to the analysis. Section 3 presents a detailed analysis of the photometry and RVs in order to determine the system characteristics. In Section 4 we discuss the discovery within the context of the known exoplanet population and the prospects for further observations.

2. TESS Observations

The star HD 118203 (see Table 1 for additional names) was observed by TESS in Sectors 15 and 16 of the mission. The star was selected for 2 minute TESS observations for several reasons. It was included in the exoplanet candidate target list accompanying version 8 of the TESS Input Catalog (TIC) of prime targets for TESS discovery of small exoplanets (Stassun et al. 2019) at a priority of 0.00282, placing it among the top 20% of targets selected for transit detection. In addition, the target was proposed for observations by a number of guest investigators.[31] Furthermore, HD 118203 was included in the Asteroseismic Target List (Schofield et al. 2019) of solar-like oscillators to be observed in 2-minute cadence with TESS. The Asteroseismic Target List comprises of bright, cool main-sequence and subgiant stars and forms part of the larger target list proposed by the TESS Asteroseismic Science Consortium.

TESS obtained 17,839 observations of HD 118203 in 2 minute cadence from 2019 August 15 to September 11, and 16,645 observations from September 11 to October 7. As a 2 minute target, the light curve was processed by the Science Processing Operations Center (SPOC) data reduction pipeline (Jenkins et al. 2016), and released through the TESS page of the Mikulski Archive for Space Telescopes (MAST).[32] The SPOC light curve clearly shows eight complete transits, and one partial transit, at a period corresponding to the ~6.13 day known planet orbital period detected by da Silva et al. (2006b).

Table 1
Literature and Measured Properties for HD 118203

Other Identifiers			
HIP 66192, Gaia 1560420854826284928			
2MASS J13340254+5343426, TYC 3850-458-1			
BD+54 1609, TIC 286923464, TOI 1271.01			
Parameter	Description	Value	Source
α_{J2000}	Right ascension (R.A.)	13:34:02.3894	1
δ_{J2000}	Declination (decl.)	+53:43:41.4752	1
l	Galactic longitude	109.°3442934	2
b	Galactic latitude	+62.°2614278	2
NUV	GALEX *NUV* mag	14.0481 ± 0.0059	3
FUV	GALEX *FUV* mag	20.16 ± 0.20	3
B_T	Tycho B_T mag	8.903 ± 0.03	4
V_T	Tycho V_T mag	8.135 ± 0.03	4
G	Gaia G mag	7.8925 ± 0.05	1
J	2MASS J mag	6.861 ± 0.021	5
H	2MASS H mag	6.608 ± 0.038	5
K_S	2MASS K_S mag	6.543 ± 0.023	5
WISE1	WISE1 mag	6.472 ± 0.078	6
WISE2	WISE2 mag	6.450 ± 0.023	6
WISE3	WISE3 mag	6.501 ± 0.016	6
WISE4	WISE4 mag	6.438 ± 0.054	6
μ_α	Gaia DR2 proper motion in R.A. (mas yr^{-1})	−85.877 ± 0.052	1
μ_δ	Gaia DR2 proper motion in decl. (mas yr^{-1})	−78.913 ± 0.038	1
π	Gaia parallax (mas)	10.892 ± 0.028[a]	1
RV	Systemic radial velocity	−29.387 ± 0.006	7
d	Distance (pc)	91.811 ± 0.236[a]	2
[Fe/H]	Iron abundance (dex)	0.23 ± 0.08	8
[C/H]	Carbon abundance (dex)	0.31 ± 0.22	8
[O/H]	Oxygen abundance (dex)	0.30 ± 0.17	8
[Mg/H]	Magnesium abundance (dex)	0.24 ± 0.12	8
[Si/H]	Silicon abundance (dex)	0.22 ± 0.14	8
[α/H]	α-element (O, Mg, Si, Ca, and Ti) abundance (dex)	0.25 ± 0.10	8
U[b]	Space velocity (km s^{-1})	4.87 ± 0.03	Section 3.5
V	Space velocity (km s^{-1})	−45.04 ± 0.12	Section 3.5
W	Space velocity (km s^{-1})	1.63 ± 0.06	Section 3.5

Notes.
[a] Values have been corrected for the −82 μas offset as reported by Stassun et al. (2019).
[b] U is in the direction of the Galactic center.
References. (1) Gaia Collaboration et al. (2018), (2) Stassun et al. (2019), (3) Bianchi et al. (2017), (4) Høg et al. (2000), (5) Cutri et al. (2003), (6) Cutri et al. (2014), (7) da Silva et al. (2006b), (8) Hypatia Catalog (Hinkel et al. 2014; www.hypatiacatalog.com).

[31] G022197 (A. Shporer), G022053 (S. Kane), and G022103 (D. Huber).

[32] https://archive.stsci.edu/tess/

During the automated search for new planets, transits of HD 118203 were identified by the SPOC transit search pipeline (Jenkins 2002; Jenkins et al. 2010), and HD 118203 was identified as a promising transit candidate by the TESS vetting procedure (N. Guerrero et al. 2020, in preparation) using TESS data validation tools (Twicken et al. 2018; Li et al. 2019) and assigned TOI number 1271.01.

The discovery paper by da Silva et al. (2006b) provides 43 individual RV observations from the ELODIE spectrograph (Baranne et al. 1996), acquired between 2004 May and 2005 July. That paper reports an orbital period for the companion of $P = 6.1335 \pm 0.0006$ days and an eccentricity of $e = 0.309 \pm 0.014$, with an additional acceleration of $49.7 \pm 5.7\,\mathrm{m\,s^{-1}\,yr^{-1}}$, and an average radial velocity of -29.387 ± 0.006 $\mathrm{km\,s^{-1}}$. Furthermore, 13 additional ELODIE RV observations taken between 2006 March and June are listed in the Data & Analysis Center for Exoplanets (DACE) data repository.[33] We have included all those RV observations in our analysis below in Section 3.

3. System Analysis

In addition to the TESS photometry and the RV data and system parameters reported by da Silva et al. (2006b), we have gathered various properties of HD 118203 from existing catalogs and archives. These include elemental abundances, spectroscopic parameters, other measures of photometric variability, and kinematic information. Those data and parameters are described below, in addition to the procedures we used to conduce a global fit of the system properties.

3.1. Abundances and Effective Temperature

A total of 37 elements (including neutral and singly ionized) were measured based on the spectrum of the host star HD 118203 by eight different groups (Gonzalez et al. 2010a, 2010b; Brugamyer et al. 2011; Maldonado et al. 2013, 2018; Delgado Mena et al. 2015; Maldonado & Villaver 2016; Luck 2017). The star is, in general, metal-rich compared with the Sun, such that only a few elemental abundance ratios fall below solar ratios ([Li/H], [Cr II/H], and [La II/H]). The median of all [Fe/H] measurements, including the determination by Sousa et al. (2015), yield a value of 0.23 ± 0.08 dex, where the uncertainty represents the spread or range in abundance measurements by the different literature sources (see Hinkel et al. 2014 for more details). In terms of important planet forming materials, the median values[34] for [C/H], [O/H], [Mg/H], and [Si/H] are listed in Table 1, which have been normalized to the solar values of Lodders et al. (2009). Also, the overall $[\alpha/\mathrm{H}]$ abundance for this planetary system, when utilizing the abundances from O, Mg, Si, Ca, and Ti, is 0.25 ± 0.10 dex. Converting to molar fractions, we find that the C/O ratio for this system is 0.47.

In addition, we utilized the stellar atmospheric determinations from the previously cited spectroscopic studies to compile an estimate of the effective temperature of HD 118203. The median of the reported $T_{\rm eff}$ values is 5816 ± 90 K, where again the uncertainty represents the spread in the effective temperature measurements. SIMBAD lists this star as a spectral type K0 dwarf based on the update of the Henry Draper Catalog (Cannon & Pickering 1993), and that spectral type appears to be repeated through a number of star catalogs. We find that the star is more appropriately considered as an early G-type. Furthermore, as the global analysis below indicates, the surface gravity of the star places it closer to the subgiant than the dwarf regime.

3.2. Global Analysis

We determined the parameters and uncertainties of the HD 118203 planetary system using the publicly available exoplanet fitting suite, EXOFASTv2 (Eastman et al. 2013, 2019). We conducted a preliminary fit of the system with EXOFASTv2 to obtain an approximate measure of the stellar surface gravity, and used a loose prior on the surface gravity of the host star of $\log g = 4.0 \pm 0.25$. We then fit the full range of available broadband photometry listed in Table 1, to a model spectral energy distribution (SED). For the SED fit, we placed a Gaussian prior on the metallicity using the value of [Fe/H] (0.23 ± 0.08 dex) from the available stellar spectra (see Section 3.1) and the corrected Gaia parallax (see Section 3.5). We also constrain the maximum line-of-sight extinction using the dust maps of Schlegel et al. (1998). The resulting SED fit provides values for $T_{\rm eff} = 5703$ K and $R_\star = 2.113\,R_\odot$.

We then placed Gaussian priors on $T_{\rm eff}$, [Fe/H], and $R_\star$ for the full EXOFASTv2 analysis using the values listed above. The error limits for stellar effective temperature and thus radius are set by the accuracy of interferometric angular diameters, which show systematic differences in excess of 3% (e.g., White et al. 2018). We therefore adopted fractional errors of 1.5% for $T_{\rm eff}$ and 3.5% for stellar radius, yielding priors of $T_{\rm eff} = 5703 \pm 86$ K and $R_\star = 2.113 \pm 0.074$ $R_\odot$ for the input to the global EXOFASTv2 fit.

We used EXOFASTv2 to simultaneously model the archival ELODIE RVs, TESS photometry, and constraints on the stellar parameters from spectroscopy. Within the fit, the stellar parameters of HD 118203 were determined using the MESA Isochrones and Stellar Tracks (MIST) stellar evolution models (Paxton et al. 2011, 2013, 2015; Choi 2016; Dotter 2016).

We fit the TESS light curve processed by the SPOC pipeline's Presearch Data Conditioning (PDC) module, which removes common-mode instrumental systematics from light curves (Smith et al. 2012; Stumpe et al. 2012, 2014). Given the very large TESS pixels of approximately 20.″25, we checked to verify that the TESS light curve is not significantly contaminated by flux from nearby stars in the TESS aperture. The TESS light curve analysis from SPOC provides a measure of the estimated crowding, via the header keyword CROWDSAP. The crowding is provided as a ratio of the flux in the aperture from the target star to the total flux in the aperture. For Sector 15, that ratio is 0.999840, and for Sector 16 that ratio is 0.999892, essentially indicating that the fraction of flux from other sources is below 0.02% of the total flux. There are also no nearby bright stars. The closest stars according to the TIC are all over 30″ away from HD 118203, and are between 10 and 12 mag fainter in the TESS bandpass. The closest star of significant brightness is 127″ away (6.3 TESS pixels), and 3.3 mag fainter.

The PDC light shows some low-frequency variability (likely originating from the rotation modulations in the light curve, see Section 3.3), which must be accounted for in transit modeling. It is particularly challenging to remove the low-frequency variability from the HD 118203 light curve because not all of the transits have sufficient out-of-transit coverage to determine and extrapolate the variability. One of the nine transits ended

[33] https://dace.unige.ch

[34] Individual abundance measurements can be found in the Hypatia Catalog: www.hypatiacatalog.com.

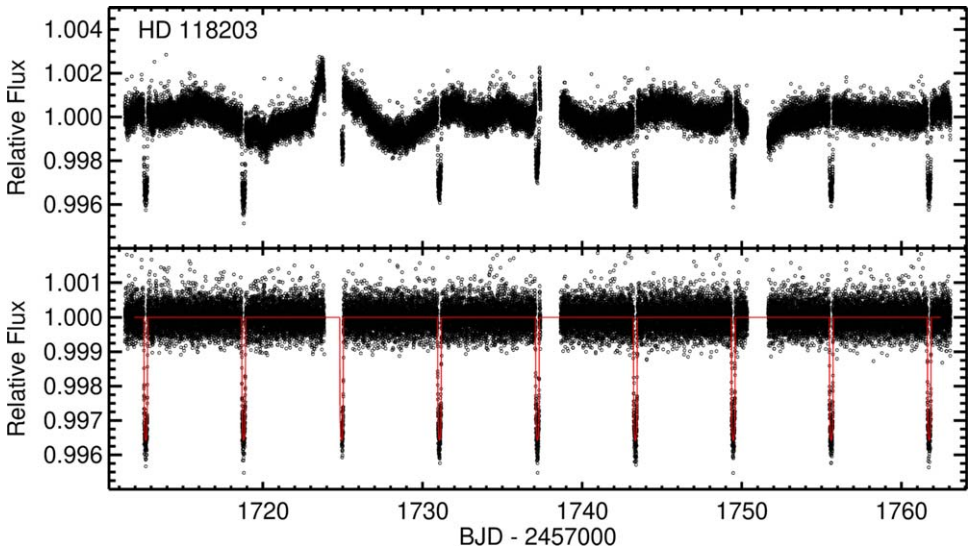

Figure 1. Top: TESS PDCSAP 2-minute cadence light curve of HD 118203 from Sectors 15 and 16. Bottom: the flattened TESS light curve used in the EXOFASTv2 fit. The observations are plotted in open black circles, and the best-fit model from EXOFASTv2 is plotted in red.

(The data used to create this figure are available.)

less than two hours before the end of Sector 15, and TESS only observed the second half of another transit after a gap in observations when the spacecraft downlinked data during its perigee passage. We chose to model the low-frequency variability with a basis spline.

We started by fitting a basis spline to the full TESS light curve, while iteratively identifying and excluding 3σ outliers (Vanderburg & Johnson 2014). We determined the optimal spacing between spline knots to be about 0.3 days by calculating the Bayesian information criterion for a series of splines fit with different knot spacings (Shallue & Vanderburg 2018). Then, we followed a procedure similar to that of Vanderburg et al. (2016), wherein we simultaneously fit the shape of the transits and the low-frequency variability (though we did not also model spacecraft systematics as is commonly done for K2 data). In brief, we performed a preliminary fit of the unflattened HD 118203 light curve with a Mandel & Agol (2002) model. Inside the fit, after each evaluation of the Mandel & Agol (2002) model, we fit a spline to the residuals (light curve–transit model) and subtracted it before calculating χ^2, which we minimized with a Levenberg–Marquardt algorithm (Markwardt 2009). After convergence, we retrieved the best-fitting spline and subtracted it from the TESS light curve, yielding a flattened light curve for the EXOFASTv2 analysis.

The SPOC PDC light curve before and after the flattening procedure is shown in Figure 1. A phase-folded zoom-in on the transit in the flattened light curve is shown in Figure 2. We show the full and phase-folded RV curve in Figure 3.

The results of the EXOFASTv2 global fit are listed in Tables 2 and 3. We note that the mass and age of the HD 118203 are bimodal in our probability distribution function (PDF; see Figure 4). The two peaks in the PDF are centered at a host star mass of 1.251 $M_{\odot}$ and 1.481 $M_{\odot}$, corresponding to ages of 5.32 Gyr and 2.87 Gyr, respectively. In order to arrive at distinct solutions, we split the host star mass PDF at the valley between the two peaks, 1.40 $M_{\odot}$, and extract two separate solutions that are presented in Tables 2 and 3. We adopt the peak at 1.251 $M_{\odot}$ since it is significantly more

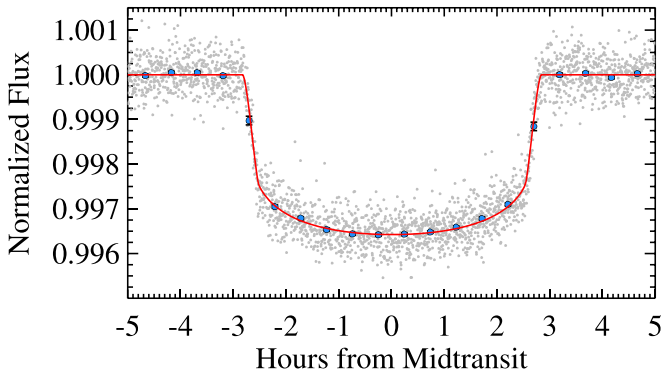

Figure 2. TESS SPOC PDC light curve of HD 118203 phase-folded to the best-fit period of 6.135 days. The blue points are showing the TESS photometry in 24 minute bins. The EXOFASTv2 model is plotted in red.

probable than the 1.481 $M_{\odot}$ solution (86.3% compared to 13.7%). However both solutions are provided in Tables 2 and 3 for future work on HD 118203. We note that the host star mass and age solutions are based on a single model grid and thus do not account for systematic errors due to different input physics, which can be substantial for evolved stars (J. Tayar et al. 2020, in preparation). Therefore, the uncertainties in mass and age reported in Table 2 are likely underestimated.

As an additional check on the system parameters, we employed the Bayesian code PARAM (Rodrigues et al. 2014, 2017; da Silva et al. 2006a) to determine fundamental properties of HD 118203 following a grid-based approach, whereby observed quantities (namely, $T_{\rm eff}$, [Fe/H], π, and apparent magnitudes) were matched to a well-sampled grid of stellar evolutionary tracks. The optimization method we adopted, the so-called 1-step approach, takes into account the entire set of input parameters at once in order to compute the PDFs for the stellar properties. This method is an updated version of the Rodrigues et al. (2014) implementation, in which the code considers both the apparent and model-derived absolute magnitudes, as part of an additional step, to derive

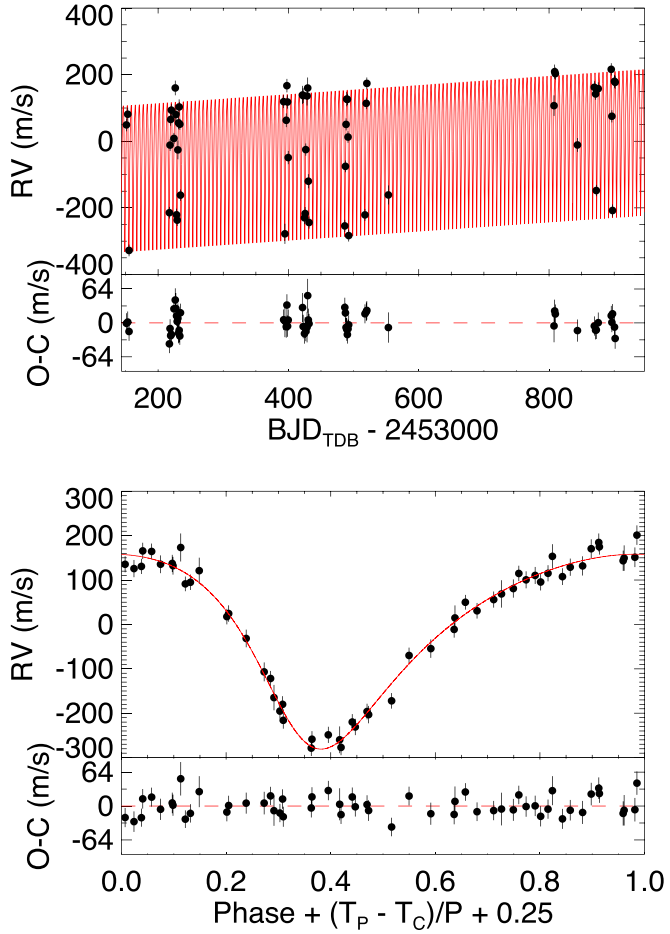

Figure 3. Top: RV measurements from ELODIE of HD 118203 (da Silva et al. 2006b). Bottom: RV measurements phase-folded to the best determined period by EXOFASTv2, 6.135 days. The EXOFASTv2 best-fit model is shown in red and the residuals of the model are shown below each plot.

the extinction and distance to the star (2-step approach). The underlying grid of stellar evolutionary tracks (and relevant physical inputs) on which we ran PARAM is described in Section 2 of Rodrigues et al. (2017). Element diffusion has, however, now been included (leading to a different He-enrichment ratio of $\Delta Y/\Delta Z = 1.33$, where Y and Z are respectively the initial helium and metal mass fractions). We note that the PARAM output is consistent with the adopted EXOFASTv2 solution.

In addition to using EXOFASTv2 to model the system, we performed an additional analysis of the TESS light curve and ELODIE RV data using `allesfitter` (Günther & Daylan 2019, 2020). `allesfitter` is an analysis framework that allows the orbital and dynamical parameters of a multi-body system to be inferred given some RV and photometric data. In this work, we omit a complete discussion of `allesfitter` and we refer the reader to Günther et al. (2019, 2020) and Daylan et al. (2019) for its implementation details. Using a Gaussian process to model the background as part of this analysis, we find a radius ratio of 5.50% ± 0.02 and an eccentricity of 0.28 ± 0.03. Although we select the EXOFASTv2 results as the final system solution, the fact that the system parameters found by `allesfitter` are in agreement is an additional verification of the robustness of the global fit.

Table 2
Median Values and 68% Confidence Intervals for the Global Model of HD 118203

Parameter	Units	Values (Adopted Solution)	Values (Secondary Solution)
Stellar Parameters:			
Probability		86.3%	13.7%
M_*	Mass ($M_\odot$)	$1.251^{+0.053}_{-0.059}$	$1.481^{+0.045}_{-0.042}$
R_*	Radius ($R_\odot$)	$2.102^{+0.052}_{-0.051}$	$2.182^{+0.049}_{-0.047}$
L_*	Luminosity ($L_\odot$)	$4.15^{+0.35}_{-0.33}$	$4.71^{+0.36}_{-0.33}$
ρ_*	Density (cgs)	0.190 ± 0.011	$0.201^{+0.011}_{-0.010}$
$\log g$	Surface gravity (cgs)	$3.889^{+0.017}_{-0.018}$	3.931 ± 0.015
$T_{\rm eff}$	Effective temperature (K)	5683^{+84}_{-85}	5757^{+81}_{-80}
A_V	V-band extinction (mag)	$0.022^{+0.014}_{-0.015}$	
[Fe/H]	Metallicity (dex)	0.223 ± 0.076	$0.264^{+0.073}_{-0.069}$
$[Fe/H]_0$[a]	Initial metallicity	$0.223^{+0.072}_{-0.074}$	$0.284^{+0.066}_{-0.059}$
Age	Age (Gyr)	$5.32^{+0.96}_{-0.73}$	2.87 ± 0.31
EEP[b]	Equal evolutionary phase	$457.4^{+4.1}_{-3.5}$	$407.6^{+5.1}_{-6.4}$
$\dot{\gamma}$	RV slope ($m\,s^{-1}\,day^{-1}$)	0.139 ± 0.012	0.138 ± 0.012

Notes.
[a] The initial metallicity is the metallicity of the star when it was formed.
[b] The equal evolutionary phase corresponds to static points in a star's evolutionary history when using the MIST isochrones and can be a proxy for age. See Section 2 in Dotter (2016) for a more detailed description of equal evolutionary phase.

3.3. Stellar Variability

To search for signs of stellar variability, we inspected the SPOC Simple Aperture Photometry version (Twicken et al. 2010; Morris et al. 2017) of the TESS light curve from Sectors 15 and 16. The initial variability analysis was performed visually, and supplemented later using the Lomb–Scargle periodogram (Lomb 1976; Scargle 1982) and the autocorrelation method (McQuillan et al. 2014). All three methods indicate that the variability is likely periodic with an estimated period of 20 ± 5 days and a semi-amplitude of about 0.2%. The largest contributor to the period uncertainty is the reduced coherency of the variability signal, indicative of potential starspot evolution (e.g., Giles et al. 2017).

The spectroscopically measured projected rotational velocity of the host star of 4.7 km s^{-1} (da Silva et al. 2006b), coupled with the newly obtained stellar radius of 2.1 $R_\odot$ (see Table 2), implies a stellar rotational period of 22 days under the assumption that the stellar rotation axis is orthogonal to the line of sight. This supports the inference that the observed variability could be caused by the stellar rotation and the presence of starspots.

HD 118203 was also observed by the Kilodegree Extremely Little Telescope (KELT), with the KELT-North Telescope (Pepper et al. 2007) between 2012 February 19 and 2014 December 30, which provided a total of 4221 photometric data points. We performed a Lomb–Scargle analysis on KELT photometry and did not detect any periodic astrophysical signals with a semi-amplitude upper limit of 24 ppt, equal to the standard deviation of the raw KELT light curve. Given that the apparent variability amplitude from the TESS photometry is

Table 3
Median Values and 68% Confidence Intervals for the Global Model of HD 118203

Parameter	Description (Units)	Values (Adopted Solution)	Values (Secondary Solution)
Probability		86.3%	13.7%
P	Period (days)	$6.134985^{+0.000029}_{-0.000030}$	6.134993 ± 0.000030
R_P	Radius (R_J)	$1.136^{+0.029}_{-0.028}$	$1.178^{+0.027}_{-0.026}$
M_P	Mass (M_J)	$2.166^{+0.074}_{-0.079}$	$2.426^{+0.066}_{-0.062}$
T_C	Time of conjunction (BJD_{TDB})	$2458712.66147^{+0.00021}_{-0.00022}$	$2458712.66145 \pm 0.00020$
T_0[a]	Optimal conjunction time (BJD_{TDB})	$2458737.20142^{+0.00017}_{-0.00019}$	$2458737.20143^{+0.00015}_{-0.00016}$
a	Semimajor axis (au)	$0.07071^{+0.00099}_{-0.0011}$	$0.07479^{+0.00074}_{-0.00071}$
i	Inclination (degrees)	$88.88^{+0.77}_{-0.97}$	$89.19^{+0.57}_{-0.82}$
e	Eccentricity	0.314 ± 0.017	0.304 ± 0.017
ω_*	Argument of Periastron (degrees)	152.8 ± 3.1	$154.9^{+3.2}_{-3.1}$
T_{eq}	Equilibrium temperature (K)	1494 ± 25	1499^{+26}_{-25}
τ_{circ}	Tidal circularization timescale (Gyr)	12.4 ± 1.3	$13.0^{+1.3}_{-1.2}$
K	RV semi-amplitude (m s^{-1})	$218.0^{+4.4}_{-4.3}$	$217.4^{+4.3}_{-4.1}$
$\log K$	Log of RV semi-amplitude	$2.3384^{+0.0086}_{-0.0087}$	$2.3372^{+0.0085}_{-0.0084}$
R_P/R_*	Radius of planet in stellar radii	$0.05552^{+0.00019}_{-0.00017}$	$0.05549^{+0.00017}_{-0.00016}$
a/R_*	Semimajor axis in stellar radii	$7.23^{+0.13}_{-0.14}$	7.37 ± 0.13
δ	Transit depth (fraction)	$0.003083^{+0.000021}_{-0.000018}$	$0.003079^{+0.000019}_{-0.000017}$
τ	Ingress/egress transit duration (days)	$0.01260^{+0.00043}_{-0.00015}$	$0.012525^{+0.00030}_{-0.000092}$
T_{14}	Total transit duration (days)	$0.23543^{+0.00056}_{-0.00048}$	$0.23537^{+0.00051}_{-0.00046}$
T_{FWHM}	FWHM transit duration (days)	$0.22274^{+0.00043}_{-0.00042}$	$0.22276^{+0.00044}_{-0.00041}$
b	Transit Impact parameter	$0.111^{+0.095}_{-0.076}$	$0.084^{+0.085}_{-0.059}$
b_S	Eclipse impact parameter	$0.15^{+0.13}_{-0.10}$	$0.109^{+0.11}_{-0.076}$
τ_S	Ingress/egress eclipse duration (days)	$0.01705^{+0.00082}_{-0.00066}$	$0.01638^{+0.00066}_{-0.00058}$
$T_{S,14}$	Total eclipse duration (days)	0.312 ± 0.011	$0.3038^{+0.0099}_{-0.010}$
$T_{S,FWHM}$	FWHM eclipse duration (days)	$0.295^{+0.011}_{-0.010}$	$0.2873^{+0.0095}_{-0.0098}$
$\delta_{S,3.6\ \mu m}$	Blackbody eclipse depth at 3.6 μm (ppm)	$228.2^{+8.3}_{-8.0}$	$225.8^{+8.0}_{-7.6}$
$\delta_{S,4.5\ \mu m}$	Blackbody eclipse depth at 4.5 μm (ppm)	$310.2^{+9.3}_{-8.8}$	$306.8^{+8.8}_{-8.4}$
ρ_P	Density (cgs)	1.83 ± 0.12	1.84 ± 0.11
$\log g_P$	Surface gravity	$3.619^{+0.019}_{-0.020}$	3.637 ± 0.018
Θ	Safronov number	$0.2154^{+0.0070}_{-0.0068}$	$0.2077^{+0.0063}_{-0.0060}$
$\langle F \rangle$	Incident flux (10^9 erg s^{-1} cm^{-2})	$1.028^{+0.070}_{-0.066}$	$1.046^{+0.073}_{-0.065}$
T_P	Time of Periastron (BJD_{TDB})	$2458707.110^{+0.042}_{-0.039}$	$2458707.148^{+0.044}_{-0.040}$
T_S	Time of eclipse (BJD_{TDB})	$2458708.508^{+0.067}_{-0.068}$	$2458708.525^{+0.068}_{-0.067}$
T_A	Time of ascending node (BJD_{TDB})	$2458710.995^{+0.052}_{-0.053}$	$2458710.960^{+0.051}_{-0.054}$
T_D	Time of descending node (BJD_{TDB})	$2458707.345^{+0.035}_{-0.033}$	$2458707.371^{+0.034}_{-0.033}$
$e \cos \omega_*$		-0.279 ± 0.018	-0.275 ± 0.018
$e \sin \omega_*$		0.144 ± 0.016	$0.129^{+0.016}_{-0.017}$
$M_P \sin i$	Minimum mass (M_J)	$2.165^{+0.074}_{-0.079}$	$2.426^{+0.066}_{-0.062}$
M_P/M_*	Mass ratio	$0.001654^{+0.000042}_{-0.000039}$	$0.001564^{+0.000034}_{-0.000032}$
d/R_*	Separation at mid transit	$5.69^{+0.23}_{-0.22}$	$5.93^{+0.23}_{-0.22}$
P_T	a priori non-grazing transit prob	$0.1658^{+0.0067}_{-0.0063}$	$0.1593^{+0.0061}_{-0.0060}$
$P_{T,G}$	a priori transit prob	$0.1854^{+0.0074}_{-0.0071}$	$0.1781^{+0.0068}_{-0.0066}$
P_S	a priori non-grazing eclipse prob	$0.1241^{+0.0025}_{-0.0022}$	$0.1229^{+0.0022}_{-0.0021}$
$P_{S,G}$	a priori eclipse prob	$0.1387^{+0.0029}_{-0.0025}$	$0.1374^{+0.0025}_{-0.0023}$
Wavelength Parameters:		TESS	
u_1	linear limb-darkening coeff	$0.311^{+0.025}_{-0.026}$	$0.309^{+0.025}_{-0.026}$
u_2	quadratic limb-darkening coeff	0.201 ± 0.042	0.206 ± 0.041
Telescope Parameters:		ELODIE	
γ_{rel}	Relative RV offset (m s^{-1})	-29312.2 ± 3.0	-29312.4 ± 2.9
σ_J	RV jitter (m s^{-1})	$15.2^{+3.1}_{-2.7}$	$15.2^{+3.1}_{-2.6}$
σ_J^2	RV jitter variance	231^{+100}_{-74}	230^{+100}_{-73}
Transit Parameters:		TESS UT 2019-S1-51 (TESS)	
σ^2	Added variance	$0.0000000090 \pm 0.0000000026$	$0.0000000090^{+0.0000000026}_{-0.0000000025}$
F_0	Baseline flux	1.0000060 ± 0.0000058	$1.0000059^{+0.0000058}_{-0.0000059}$

Notes. See Table 3 in Eastman et al. (2019) for a list of the derived and fitted parameters in EXOFASTv2.
[a] Minimum covariance with period. All of the values in this table for the secondary eclipse of HD 118203 b are predicted values from our global analysis.

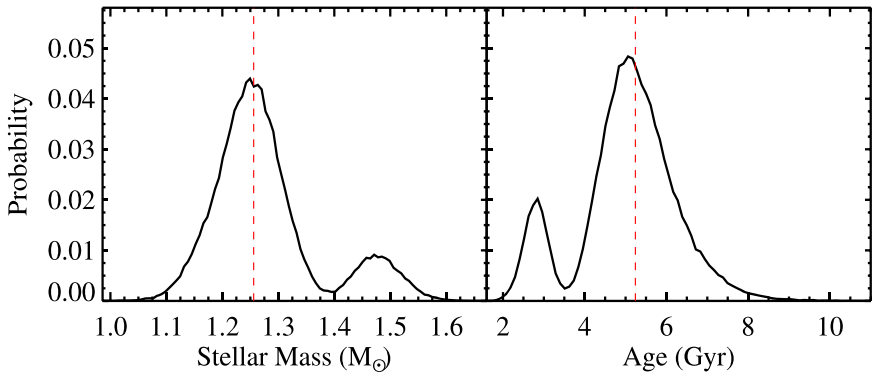

Figure 4. Probability distribution function for M_* in units of solar mass (left) and age (right). The red line shows the median value for each parameter from the adopted solution (see Section 3.2).

smaller than the detection threshold for KELT, the non-detection of both the rotation signal and the transit in KELT is unsurprising.

3.4. Search for Close Stellar Companions

The parameters of a transiting planet depend on the transit depth, which can be affected by the presence of nearby unresolved luminous companions (Ciardi et al. 2015). Furthermore, the trend in the RV data could be indicative of a distant bound companion, either a massive planet, brown dwarf, or low-mass star. Therefore, to properly account for any photometric flux contamination from unaccounted stellar sources, we conducted high spatial resolution imaging to detect any such sources.

HD 118203 was observed on 2019 December 19 UT using the 'Alopeke speckle instrument on Gemini-North.[35] 'Alopeke provides simultaneous high-resolution speckle imaging in two bands, 562 and 832 nm, with output data products including a reconstructed image, and robust limits on companion detections (Howell et al. 2011). Three sets of 1000 60 ms images each were combined to provide the final speckle results. Figure 5 shows the 562 nm (green) and 832 nm (red) 5σ contrast curves and a zoomed-in view of the 832 nm reconstructed speckle image (0.″31 on a side). From the speckle images, we find that HD 118203 has no companion brighter that about 4–9 mag detected within 1.″25.

We combine the speckle imaging results and the slope of the RV time series to constrain the properties of the possible companion following the methods from Kane et al. (2019). The RV slope provides lower limits on the combined mass and separation of a companion. We treat the lower limit of the semi-amplitude (K) as $(t_f - t_0) * \dot{\gamma}/2$, where t_0 and t_f are the timing of first and last RV epoch, respectively, and $\dot{\gamma}$ is the slope of the RV time series. Then, we numerically solve the following relation for the companion minimum mass (M_p) as a function of semimajor axis (a):

$$K \leqslant \sqrt{\frac{G}{a(1-e^2)}} \frac{M_p \sin i}{\sqrt{M_\star + M_p}}, \quad (1)$$

where G is the gravitational constant, e is the companion orbital eccentricity, and i is the companion orbital inclination. We take a Monte Carlo approach to account for the unknown companion eccentricity and inclination. As a function of semimajor axis, we evaluate the above relation 1000 times drawing inclination from a uniform distribution in $\cos i$ and drawing eccentricity from a Beta distribution with shape parameters $\alpha = 0.867$ and $\beta = 3.03$ (Kipping 2013). The speckle imaging observations in each band correspond to upper limits on the mass of a companion. We apply the technique of Kane et al. (2014), which we briefly summarize here. Using the distance to HD 118203 and the mass–luminosity relations of Henry & McCarthy (1993), we estimate the apparent V-band magnitude of a possible stellar companion as a function of M_p. Comparison to the known apparent V-band magnitude of HD 118203 yields visual Δm, also as a function of M_p. We convert these to speckle Δm values using the Pickles spectral library (Pickles 1998) and the filter transmission curves. Finally, we compare these to the 5σ speckle imaging limiting magnitude curves to find M_p as a function of angular separation.

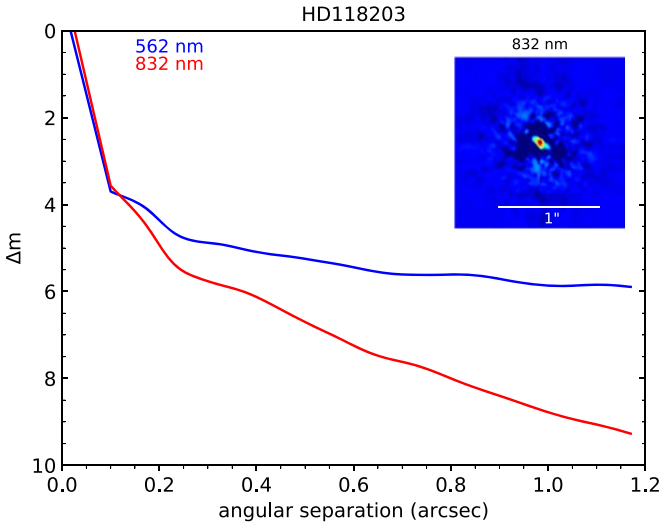

Figure 5. Contrast curves from speckle imaging of HD 118203, with an inset of the speckle image in the 832 nm channel. No luminous companions are detected.

The results are shown in Figure 6. The plot displays both upper mass limits from the speckle imaging, and the lower mass limits from the RV slope. Since any bound companions would have to be in the low-mass stellar regime, the 832 nm speckle data provides stronger constraints than the 562 nm data. We see that if a companion is the cause of the RV trend, it is likely to be a late-type M-dwarf star or brown dwarf.

[35] https://www.gemini.edu/sciops/instruments/alopeke-zorro/

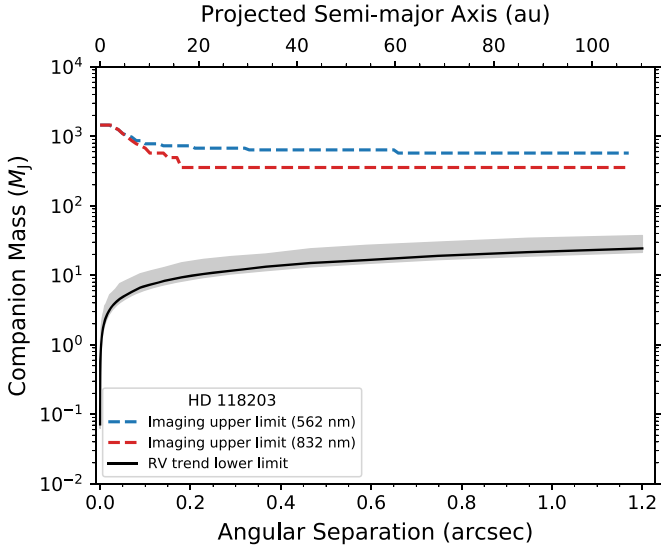

Figure 6. Constraints on the mass of an undetected bound outer companion to HD 118203 from speckle limits and the RV trend. The gray band shows the 1σ errors on the RV limits based on Monte Carlo sampling of the possible companion eccentricity and inclination.

3.5. Location and Kinematics in the Galaxy

HD 118203 is labeled as a high-proper motion star by SIMBAD. This could be due to the fact that it is relatively close, or it could be because it has a higher than average space velocity for a typical thin disk star (which might imply that it is older than the typical age of the thin disk or a member of the thick disk), or some combination of the two. To determine the location and kinematics of HD 118203, we use the Gaia parallax (corrected for the 82 μas systematic according to Stassun & Torres 2018) and the Gaia proper motions and parallax (Gaia Collaboration et al. 2018).

The corrected parallax is 10.892 ± 0.028 mas, which implies a distance from the Sun of 91.811 ± 0.236 pc.[36] The Galactic coordinates of HD 118203 are $(\ell, b) = (109.^\circ34, +62.^\circ3)$, and thus the difference in the vertical position of HD 118203 from that of the Sun is Z–$Z_\odot = 81$ pc. Given the $Z_\odot \simeq 30$ pc determined from giants in the local solar neighborhood (Bovy 2017), we find $Z \simeq 111$ pc. This is comparable to the scale height of early G stars in the local Galactic disk as determined by Bovy (2017). Given the relatively small distance of HD 118203 from the Sun and the fact that it is located at roughly $\ell \sim 90^\circ$, we find that the Galactocentric distance of HD 118203 is essentially the same as that of the Sun (to within $\lesssim$1%).

We determine the space velocity of HD 118203 to be $(U, V, W) = (4.87 \pm 0.03, -45.04 \pm 0.12, 1.63 \pm 0.06)$ km s^{-1}, correcting for the velocity of the Sun with respect to the local standard of rest as determined by Coşkunoğlu et al. (2011). Thus HD 118203 has relatively small U and W velocities relative to the dispersion in the local disk, but a relatively high asymmetric drift. This generally indicates a relatively old (but still thin disk) star, which would not be surprising given that it is a mid-type star. The classification scheme of Bensby et al. (2003) gives a 97.5% chance that this is a thin disk star. This is corroborated by the abundances, [Fe/H] $= 0.23 \pm 0.08$ and [α/Fe] $=0.25 \pm 0.10$.

[36] Given the very small ($\sim$0.3%) fractional uncertainty in the parallax, we do not attempt to correct for Lutz–Kelker bias (Lutz & Kelker 1973).

4. Discussion

4.1. Demographic Properties

The fact that HD 118203 b orbits such a bright host star makes this an exciting representative of a transiting planet. Out of the 3074 confirmed planets listed on the NASA Exoplanet Archive[37] that are not labeled as "controversial," that are known to transit, and that have a host star with a recorded optical magnitude, HD 118203 is brighter than all but 12 host stars, and is the eighth brightest transit host in the northern hemisphere.

Additionally, HD 118203 b is a massive transiting planet in a short-period, eccentric orbit. That combination of properties is shown in Figures 7 and 8, which display all known transiting planets in orbits with significant eccentricity ($e > 0.05$). HD 118203 b is one of the few transiting planets in eccentric orbits with a bright host star.

4.2. Expectations for Transits of RV-detected Planets

By observing bright stars covering almost the entire sky, TESS offers a unique opportunity to search for transits of exoplanets that were discovered via RV variations of their host stars. Considering the geometric transit probability of each RV-detected system and the observational strategy of TESS, Dalba et al. (2019) predicted that TESS would observe transits for $\sim$11 RV-detected planets in its primary mission. However, only three of these detections were expected to be novel, such that the RV-detected planet was not previously known to transit.

The discovery of transits for HD 118203 b at approximately halfway through the TESS primary mission is consistent with this prediction. If the detection rate is (roughly) one per cycle, then we should expect one more discovery by the end of Cycle 2. As is the case with HD 118203 b, any other RV-detected planets found to transit are likely to have short-period orbits compared to the average RV-detected planet.

Since the orbital period of HD 118203 b is shorter than the duration of a TESS sector, its a priori transit probability is not reduced due to the observational baseline. The a priori geometric transit probability of HD 118203 b is 0.21 ± 0.02 (Dalba et al. 2019), placing it in the 98th percentile among all RV-detected exoplanets. The a posteriori transit probability (Stevens & Gaudi 2013) may be higher; however this depends on the true mass distribution of planets with masses within a factor of a few of HD 118203 b. Based on the fact that, from RV surveys, it is known that companions with minimum masses somewhat larger than that of Jupiter on relatively short-period ($P \lesssim$ a few years) orbits appear to have a mass function that decreases with increasing mass, at least until the "driest" part of the brown dwarf desert (Grether & Lineweaver 2006), the a posteriori transit probability is likely to be higher for planets in this minimum mass regime than the naive a priori transit probability (Stevens & Gaudi 2013) would suggest. Indeed, the population synthesis models used by Stevens & Gaudi (2013) to determine the scale factor that relates the a posteriori and a priori transit probabilities suggest that HD 118203 b is right on the boundary of having a significant boost in the probability of transit relative to the naive a priori estimate. In general, we follow Stevens & Gaudi (2013) and suggest that targeting RV-detected planets with minimum mass

[37] https://exoplanetarchive.ipac.caltech.edu, queried on 2019 October 14.

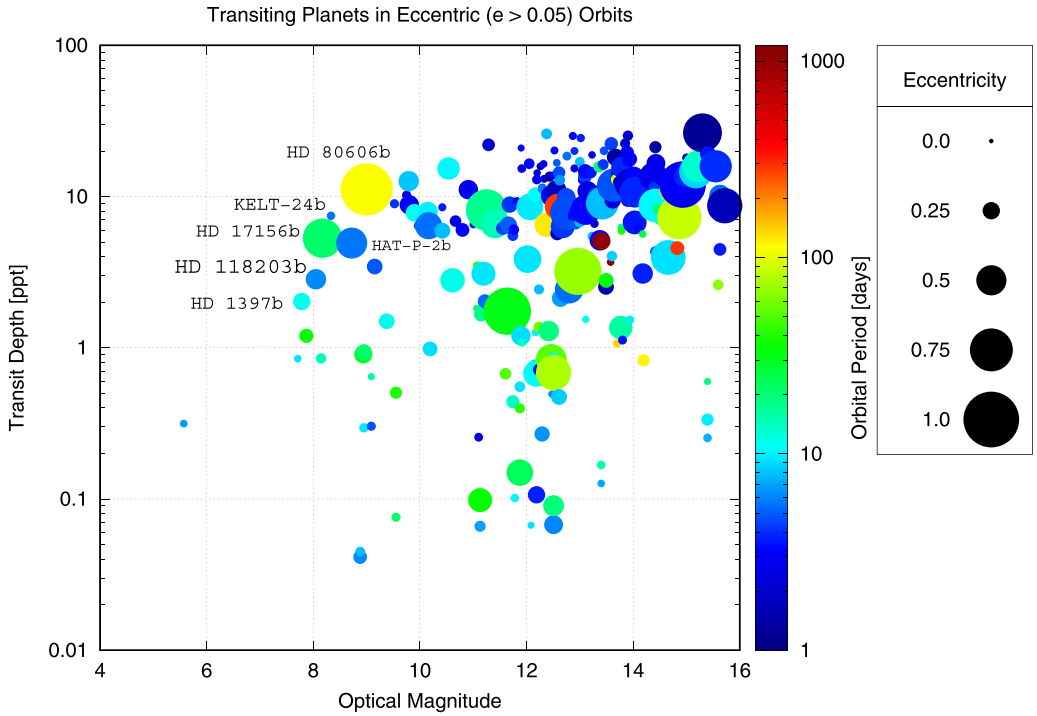

Figure 7. All known transiting planets in orbits with eccentricity greater than 0.05. HD 118203 b occupies a spot in the upper left of the distribution, along with a few other transiting planets orbiting bright stars with large transit depths. Data from the NASA Exoplanet Archive, retrieved 2019 October 15.

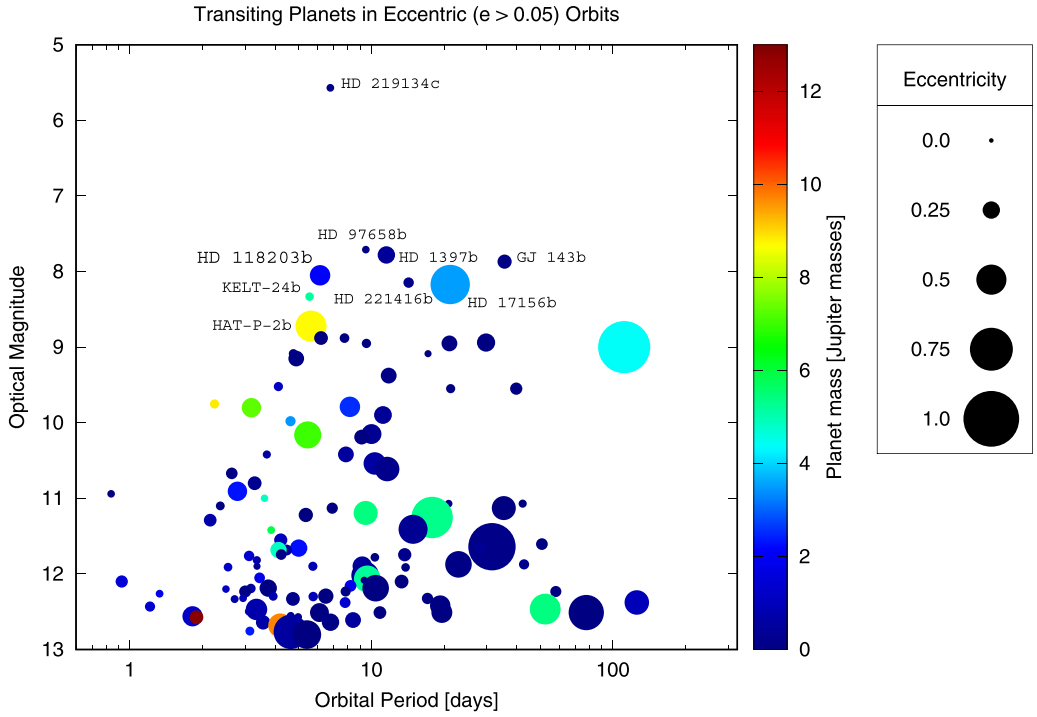

Figure 8. All known transiting planets in orbits with eccentricity greater than 0.05. HD 118203 b occupies a spot near the top of the distribution, along with a few other transiting planets orbiting bright stars. Data from the NASA Exoplanet Archive, retrieved 2019 October 15.

in the regime where the true mass function is likely decreasing sharply with increasing mass (super-Jupiters, super-Earths, and Neptunes) may result in a higher yield of transiting planets than naive a priori transit estimates would imply. There are more than 30 RV-detected exoplanets with a priori transit probabilities as observed by TESS between 0.1 and 0.3 (Dalba et al. 2019, their Table 1). Although some of these are already known to transit (e.g., 55 Cnc e), the next RV-detected exoplanet found to transit likely resides in this group, and is even more likely to be in the minimum mass regimes mentioned above. Stevens & Gaudi (2013) also provide a list of particularly promising systems with transit probabilities that are likely to be higher than naively expected (see their Table 3).

4.3. Observing Prospects

HD 118203 was observed by TESS in Sector 15 (2019 August 15 to September 11) and Sector 16 (2019 September 11 to October 7), which are the data sets we have analyzed here. It is also expected to be observed in TESS Sector 22 (2020 February 18 to March 18). While we do not expect those data to lead to significant updates to the fundamental physical parameters of the system, the additional photometry can potentially provide a more precise measurement of the orbital period of the planet.

Another exciting prospect is that the additional photometry could allow the detection of solar-like oscillations in HD 118203 using asteroseismic analysis. That is primarily due to that star's brightness of $T = 7.45$ and the fact that it is slightly evolved (see Section 3.2). HD 118203 is therefore within the regime suitable for asteroseismology described by Campante et al. (2016). The actual observability of solar-like oscillations awaits a more detailed analysis of the TESS photometry once the future sectors of observations are acquired.

The combination of a relatively short orbital period, bright host star, and eccentric orbit presents an opportunity for phase curve observations of the system. The secondary eclipse is predicted to take place 33 hr after periastron passage. Infrared observations of the system during and after periastron passage through the secondary eclipse could provide insight into the thermal properties of the planetary atmosphere and dynamics of heat transport, such as observed for HAT-P-2b (Lewis et al. 2013). Although Spitzer observations are no longer available, the James Webb Space Telescope (JWST) presents an excellent opportunity for such observations.

We would like to thank Avi Shporer and Chelsea Huang for helpful conversations.

This paper includes data collected with the TESS mission, obtained from the MAST data archive at the Space Telescope Science Institute (STScI). Funding for the TESS mission is provided by the NASA Explorer Program. STScI is operated by the Association of Universities for Research in Astronomy, Inc., under NASA contract NAS 526555.

T.D. acknowledges support from MIT's Kavli Institute as a Kavli postdoctoral fellow. A.V.'s work was performed under contract with the California Institute of Technology/Jet Propulsion Laboratory funded by NASA through the Sagan Fellowship Program executed by the NASA Exoplanet Science Institute.

D.H. acknowledges support by the National Aeronautics and Space Administration (80NSSC18K1585, 80NSSC19K0379) awarded through the TESS Guest Investigator Program and by the National Science Foundation (AST-1717000).

T.L.C. acknowledges support from the European Union's Horizon 2020 research and innovation program under the Marie Skłodowska-Curie grant agreement No. 792848 (PULSATION). This work was supported by FCT/MCTES through national funds (UID/FIS/04434/2019).

D.B. is supported in the form of work contract FCT/MCTES through national funds and by FEDER through COMPETE2020 in connection to these grants: UID/FIS/04434/2019, PTDC/FIS-AST/30389/2017, and POCI-01-0145-FEDER-030389.

P.D. is supported by a National Science Foundation (NSF) Astronomy and Astrophysics Postdoctoral Fellowship under award AST-1903811.

M.N.G. acknowledges support from MIT's Kavli Institute as a Torres postdoctoral fellow.

This work has made use of NASA's Astrophysics Data System, the SIMBAD database operated at CDS, Strasbourg, France, and the VizieR catalog access tool, CDS, Strasbourg, France. We acknowledge the use of public TESS Alert data from pipelines at the TESS Science Office and at the TESS Science Processing Operations Center. We make use of Filtergraph, an online data visualization tool developed at Vanderbilt University through the Vanderbilt Initiative in Data-intensive Astrophysics (VIDA). The research shown here acknowledges use of the Hypatia Catalog Database, an online compilation of stellar abundance data as described in Hinkel et al. (2014), which was supported by NASA's Nexus for Exoplanet System Science (NExSS) research coordination network and the Vanderbilt Initiative in Data-Intensive Astrophysics (VIDA). This research has made use of the NASA Exoplanet Archive, which is operated by the California Institute of Technology, under contract with the National Aeronautics and Space Administration under the Exoplanet Exploration Program. This publication makes use of The Data & Analysis Center for Exoplanets (DACE), which is a facility based at the University of Geneva (CH) dedicated to extrasolar planets data visualization, exchange, and analysis. DACE is a platform of the Swiss National Centre of Competence in Research (NCCR) PlanetS, federating the Swiss expertise in Exoplanet research. The DACE platform is available at https://dace.unige.ch. Based on observations obtained at the Gemini Observatory, which is operated by the Association of Universities for Research in Astronomy, Inc., under a cooperative agreement with the NSF on behalf of the Gemini partnership: the National Science Foundation (United States), National Research Council (Canada), CONICYT (Chile), Ministerio de Ciencia, Tecnología e Innovación Productiva (Argentina), Ministério da Ciência, Tecnologia e Inovação (Brazil), and Korea Astronomy and Space Science Institute (Republic of Korea). Some of the Observations in the paper made use of the High-Resolution Imaging instrument Alopeke at Gemini-North. Alopeke was funded by the NASA Exoplanet Exploration Program and built at the NASA Ames Research Center by Steve B. Howell, Nic Scott, Elliott P. Horch, and Emmett Quigley. This research made use of Astropy,[38] a community-developed core Python package for Astronomy (Astropy Collaboration et al. 2013, 2018). We also used data products from the Widefield Infrared Survey Explorer, which is a joint project of the University of California, Los Angeles; the Jet Propulsion Laboratory/California Institute of Technology, which is funded by the National Aeronautics and Space Administration; the Two Micron All Sky Survey, which is a joint project of the University of Massachusetts and the Infrared Processing and Analysis Center/California Institute of Technology, funded by the National Aeronautics and Space Administration and the National Science Foundation; and the European Space Agency (ESA) mission Gaia (http://www.cosmos.esa.int/gaia), processed by the Gaia Data Processing and Analysis Consortium (DPAC, http://www.cosmos.esa.int/web/gaia/dpac/consortium). Funding for the DPAC has been provided by national institutions, in particular the institutions participating in the Gaia Multilateral Agreement. We acknowledge support for the KELT project through the

[38] http://www.astropy.org

Vanderbilt Initiative in Data-intensive Astrophysics, Ohio State University, and Lehigh University. Part of this research was carried out at the Jet Propulsion Laboratory, California Institute of Technology, under a contract with the National Aeronautics and Space Administration (NASA). Resources supporting this work were provided by the NASA High-End Computing (HEC) Program through the NASA Advanced Supercomputing (NAS) Division at Ames Research Center for the production of the SPOC data products.

ORCID iDs

Joshua Pepper https://orcid.org/0000-0002-3827-8417
Stephen R. Kane https://orcid.org/0000-0002-7084-0529
Joseph E. Rodriguez https://orcid.org/0000-0001-8812-0565
Natalie R. Hinkel https://orcid.org/0000-0003-0595-5132
Jason D. Eastman https://orcid.org/0000-0003-3773-5142
Tansu Daylan https://orcid.org/0000-0002-6939-9211
Teo Mocnik https://orcid.org/0000-0003-4603-556X
Paul A. Dalba https://orcid.org/0000-0002-4297-5506
B. Scott Gaudi https://orcid.org/0000-0003-0395-9869
Keivan G. Stassun https://orcid.org/0000-0002-3481-9052
Tiago L. Campante https://orcid.org/0000-0002-4588-5389
Andrew Vanderburg https://orcid.org/0000-0001-7246-5438
Daniel Huber https://orcid.org/0000-0001-8832-4488
Diego Bossini https://orcid.org/0000-0002-9480-8400
Ian Crossfield https://orcid.org/0000-0002-1835-1891
Steve B. Howell https://orcid.org/0000-0002-2532-2853
Andrew W. Stephens https://orcid.org/0000-0002-4434-2307
E. Furlan https://orcid.org/0000-0001-9800-6248
George R. Ricker https://orcid.org/0000-0003-2058-6662
Roland Vanderspek https://orcid.org/0000-0001-6763-6562
David W. Latham https://orcid.org/0000-0001-9911-7388
S. Seager https://orcid.org/0000-0002-6892-6948
Joshua N. Winn https://orcid.org/0000-0002-4265-047X
Jon M. Jenkins https://orcid.org/0000-0002-4715-9460
Joseph D. Twicken https://orcid.org/0000-0002-6778-7552
Mark Rose https://orcid.org/0000-0003-4724-745X
Jeffrey C. Smith https://orcid.org/0000-0002-6148-7903
Ana Glidden https://orcid.org/0000-0002-5322-2315
Karen A. Collins https://orcid.org/0000-0001-6588-9574
Andrew W. Mann https://orcid.org/0000-0003-3654-1602
Jennifer A. Burt https://orcid.org/0000-0002-0040-6815
David J. James https://orcid.org/0000-0001-5160-4486
Robert J. Siverd https://orcid.org/0000-0001-5016-3359
Maximilian N. Günther https://orcid.org/0000-0002-3164-9086

References

Astropy Collaboration, Price-Whelan, A. M., Sipőcz, B. M., et al. 2018, AJ, 156, 123
Astropy Collaboration, Robitaille, T. P., Tollerud, E. J., et al. 2013, A&A, 558, A33
Baranne, A., Queloz, D., Mayor, M., et al. 1996, A&AS, 119, 373
Barbieri, M., Alonso, R., Laughlin, G., et al. 2007, A&A, 476, L13
Bensby, T., Feltzing, S., & Lundström, I. 2003, A&A, 410, 527
Bianchi, L., Shiao, B., & Thilker, D. 2017, ApJS, 230, 24
Bonfils, X., Gillon, M., Udry, S., et al. 2012, A&A, 546, A27
Bouchy, F., Udry, S., Mayor, M., et al. 2005, A&A, 444, L15
Bovy, J. 2017, MNRAS, 470, 1360
Brugamyer, E., Dodson-Robinson, S. E., Cochran, W. D., & Sneden, C. 2011, ApJ, 738, 97
Campante, T. L., Schofield, M., Kuszlewicz, J. S., et al. 2016, ApJ, 830, 138
Cannon, A. J., & Pickering, E. C. 1993, yCat, III/135A, 0
Charbonneau, D., Brown, T. M., Latham, D. W., & Mayor, M. 2000, ApJL, 529, L45
Choi, J., Dotter, A., Conroy, C., et al. 2016, ApJ, 823, 102
Ciardi, D. R., Beichman, C. A., Horch, E. P., & Howell, S. B. 2015, ApJ, 805, 16
Coşkunoğlu, B., Ak, S., Bilir, S., et al. 2011, MNRAS, 412, 1237
Cutri, R. M., Skrutskie, M. F., van Dyk, S., et al. 2003, yCat, 2246, 0
Cutri, R. M., et al. 2014, yCat, 2328, 0
Dalba, P. A., Kane, S. R., Barclay, T., et al. 2019, PASP, 131, 034401
da Silva, L., Girardi, L., Pasquini, L., et al. 2006a, A&A, 458, 609
da Silva, R., Udry, S., Bouchy, F., et al. 2006b, A&A, 446, 717
Daylan, T., Günther, M. N., Mikal-Evans, T., et al. 2019, arXiv:1909.03000
Delgado Mena, E., Bertrán de Lis, S., Adibekyan, V. Z., et al. 2015, A&A, 576, A69
Demory, B. O., Gillon, M., Deming, D., et al. 2011, A&A, 533, A114
Dotter, A. 2016, ApJS, 222, 8
Dragomir, D., Kane, S. R., Henry, G. W., et al. 2012, ApJ, 754, 37
Dragomir, D., Kane, S. R., Pilyavsky, G., et al. 2011, AJ, 142, 115
Dragomir, D., Matthews, J. M., Eastman, J. D., et al. 2013, ApJL, 772, L2
Eastman, J., Gaudi, B. S., & Agol, E. 2013, PASP, 125, 83
Eastman, J. D., Rodriguez, J. E., Agol, E., et al. 2019, arXiv:1907.09480
Fossey, S. J., Waldmann, I. P., & Kipping, D. M. 2009, MNRAS, 396, L16
Gaia Collaboration, Brown, A. G. A., Vallenari, A., et al. 2018, A&A, 616, A1
Garcia-Melendo, E., & McCullough, P. R. 2009, ApJ, 698, 558
Giles, H. A. C., Collier Cameron, A., & Haywood, R. D. 2017, MNRAS, 472, 1618
Gillon, M., Demory, B.-O., Van Grootel, V., et al. 2017, NatAs, 1, 0056
Gillon, M., Pont, F., Demory, B. O., et al. 2007, A&A, 472, L13
Gonzalez, G., Carlson, M. K., & Tobin, R. W. 2010a, MNRAS, 403, 1368
Gonzalez, G., Carlson, M. K., & Tobin, R. W. 2010b, MNRAS, 407, 314
Grether, D., & Lineweaver, C. H. 2006, ApJ, 640, 1051
Günther, M. N., & Daylan, T. 2019, allesfitter: Flexible star and exoplanet inference from photometry and radial velocity, Astrophysics Source Code Library, ascl:1903.003
Günther, M. N., & Daylan, T. 2020, arXiv:2003.14371
Günther, M. N., Pozuelos, F. J., Dittmann, J. A., et al. 2019, NatAs, 3, 1099
Günther, M. N., Zhan, Z., Seager, S., et al. 2020, AJ, 159, 60
Henry, G. W., Marcy, G. W., Butler, R. P., & Vogt, S. S. 2000, ApJL, 529, L41
Henry, T. J., & McCarthy, D. W. J. 1993, AJ, 106, 773
Hinkel, N. R., Kane, S. R., Henry, G. W., et al. 2015, ApJ, 803, 8
Hinkel, N. R., Timmes, F. X., Young, P. A., Pagano, M. D., & Turnbull, M. C. 2014, AJ, 148, 54
Høg, E., Fabricius, C., Makarov, V. V., et al. 2000, A&A, 355, L27
Howell, S. B., Everett, M. E., Sherry, W., Horch, E., & Ciardi, D. R. 2011, AJ, 142, 19
Huang, C. X., Burt, J., Vanderburg, A., et al. 2018, ApJL, 868, L39
Jenkins, J. M. 2002, ApJ, 575, 493
Jenkins, J. M., Chandrasekaran, H., McCauliff, S. D., et al. 2010, Proc. SPIE, 7740, 77400D
Jenkins, J. M., Twicken, J. D., McCauliff, S., et al. 2016, Proc. SPIE, 9913, 99133E
Jones, M. I., Brahm, R., Espinoza, N., et al. 2019, A&A, 625, A16
Kane, S. R. 2007, MNRAS, 380, 1488
Kane, S. R., Dalba, P. A., Li, Z., et al. 2019, AJ, 157, 252
Kane, S. R., Howard, A. W., Pilyavsky, G., et al. 2011, ApJ, 733, 28
Kane, S. R., Howell, S. B., Horch, E. P., et al. 2014, ApJ, 785, 93
Kane, S. R., Mahadevan, S., von Braun, K., Laughlin, G., & Ciardi, D. R. 2009, PASP, 121, 1386
Kane, S. R., & von Braun, K. 2008, ApJ, 689, 492
Kane, S. R., Wittenmyer, R. A., Hinkel, N. R., et al. 2016, ApJ, 821, 65
Kempton, E. M. R., Bean, J. L., Louie, D. R., et al. 2018, PASP, 130, 114401
Kipping, D. M. 2013, MNRAS, 434, L51
Knutson, H. A., Charbonneau, D., Allen, L. E., et al. 2007, Natur, 447, 183
Laughlin, G., Deming, D., Langton, J., et al. 2009, Natur, 457, 562
Lewis, N. K., Knutson, H. A., Showman, A. P., et al. 2013, ApJ, 766, 95
Li, J., Tenenbaum, P., Twicken, J. D., et al. 2019, PASP, 131, 024506
Lodders, K., Plame, H., & Gail, H.-P. 2009, LanB, 4B, 712
Lomb, N. R. 1976, Ap&SS, 39, 447
Luck, R. E. 2017, AJ, 153, 21
Lutz, T. E., & Kelker, D. H. 1973, PASP, 85, 573
Maldonado, J., & Villaver, E. 2016, A&A, 588, A98
Maldonado, J., Villaver, E., & Eiroa, C. 2013, A&A, 554, A84

Maldonado, J., Villaver, E., & Eiroa, C. 2018, A&A, 612, A93
Mandel, K., & Agol, E. 2002, ApJL, 580, L171
Markwardt, C. B. 2009, in ASP Conf. Ser. 411, Astronomical Data Analysis Software and Systems XVIII, ed. D. A. Bohlender, D. Durand, & P. Dowler (San Francisco, CA: ASP), 251
McQuillan, A., Mazeh, T., & Aigrain, S. 2014, ApJS, 211, 24
Morris, R. L., Twicken, J. D., Smith, J. C., et al. 2017, Kepler Data Processing Handbook: Photometric Analysis, Kepler Science Document KSCI-19081-002
Motalebi, F., Udry, S., Gillon, M., et al. 2015, A&A, 584, A72
Paxton, B., Bildsten, L., Dotter, A., et al. 2011, ApJS, 192, 3
Paxton, B., Cantiello, M., Arras, P., et al. 2013, ApJS, 208, 4
Paxton, B., Marchant, P., Schwab, J., et al. 2015, ApJS, 220, 15
Pepper, J., Pogge, R. W., DePoy, D. L., et al. 2007, PASP, 119, 923
Pickles, A. J. 1998, PASP, 110, 863
Pilyavsky, G., Mahadevan, S., Kane, S. R., et al. 2011, ApJ, 743, 162
Ricker, G. R., Winn, J. N., Vanderspek, R., et al. 2015, JATIS, 1, 014003
Rodrigues, T. S., Bossini, D., Miglio, A., et al. 2017, MNRAS, 467, 1433
Rodrigues, T. S., Girardi, L., Miglio, A., et al. 2014, MNRAS, 445, 2758
Rodriguez, J. E., Quinn, S. N., Huang, C. X., et al. 2019, AJ, 157, 191
Sato, B., Fischer, D. A., Henry, G. W., et al. 2005, ApJ, 633, 465
Scargle, J. D. 1982, ApJ, 263, 835
Schlegel, D. J., Finkbeiner, D. P., & Davis, M. 1998, ApJ, 500, 525
Schofield, M., Chaplin, W. J., Huber, D., et al. 2019, ApJS, 241, 12
Shallue, C. J., & Vanderburg, A. 2018, AJ, 155, 94
Smith, J. C., Stumpe, M. C., Van Cleve, J. E., et al. 2012, PASP, 124, 1000
Sousa, S. G., Santos, N. C., Mortier, A., et al. 2015, A&A, 576, A94
Stassun, K. G., Oelkers, R. J., Paegert, M., et al. 2019, AJ, 158, 138
Stassun, K. G., & Torres, G. 2018, ApJ, 862, 61
Stevens, D. J., & Gaudi, B. S. 2013, PASP, 125, 933
Stumpe, M. C., Smith, J. C., Catanzarite, J. H., et al. 2014, PASP, 126, 100
Stumpe, M. C., Smith, J. C., Van Cleve, J. E., et al. 2012, PASP, 124, 985
Twicken, J. D., Catanzarite, J. H., Clarke, B. D., et al. 2018, PASP, 130, 064502
Twicken, J. D., Clarke, B. D., Bryson, S. T., et al. 2010, Proc. SPIE, 7740, 774023
Vanderburg, A., & Johnson, J. A. 2014, PASP, 126, 948
Vanderburg, A., Latham, D. W., Buchhave, L. A., et al. 2016, ApJS, 222, 14
White, T. R., Huber, D., Mann, A. W., et al. 2018, MNRAS, 477, 4403
Winn, J. N., Matthews, J. M., Dawson, R. I., et al. 2011, ApJL, 737, L18